

pubs.acs.org/crystal Article

Discerning the Impact of Noncovalent Interactions via Simulated Crystal Growth: A Structural Study of Aromatic Esters

Mairead Boucher, Sophia A. Bellia, Alexis Howarth, Anne Collart, Muhammadiqboli Musozoda, Clinton Adu, Gary L. Guillet, Antonio Barbosa, Pasquale F. Fulvio, Arsalan Mirjafari,* Matthias Zeller, and Patrick C. Hillesheim*



Cite This: https://doi.org/10.1021/acs.cgd.3c01485



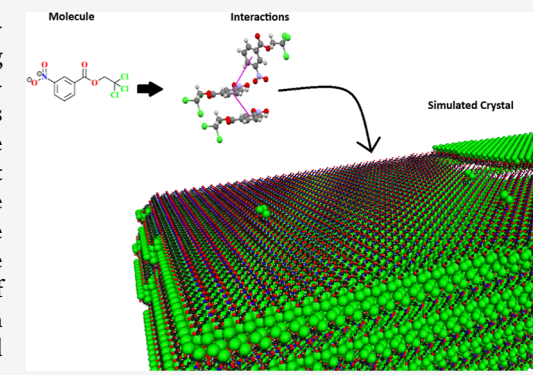
ACCESS

Metrics & More

Article Recommendations

SI Supporting Information

ABSTRACT: The synthesis and structural characterization of seven systematically varied aromatic esters are reported. The compounds are analyzed using single-crystal X-ray diffraction, dynamic scanning calorimetry, and variable-temperature viscometry. The state of the compounds, i.e., liquid and solid, is controlled, in part, via sterics of the ester functionalities which influence the presence of specific noncovalent interactions in the solid state. Two distinct conformational polymorphs are observed in the solid state. To rationalize the formation of the conformational polymorphs, the intermolecular forces of the crystalline structures were studied via Hirshfeld surface analysis, leading to the conclusion that the unique geometries are controlled by a combination of halogen contacts, π interactions, and interactions involving the nitro group on the aromatic rings. These conclusions are further examined via computational studies of the conformers, analysis of packing efficiency, and assessment of the



structure of the energy frameworks for the crystalline solids. Finally, the information derived from the analysis of the interactions is used to simulate the growth of the crystals, helping to rationalize the conclusions about which interactions are responsible for the phase behavior of the compounds.

1. INTRODUCTION

One of the fundamental principles of chemistry is that structure, or form, begets function. This statement is constant across practically every branch of chemistry from materials design to crystal engineering to function-specific applications.³ The field of molecular design is likewise impacted by this principle. Designing new materials and understanding their function using established structure-property relationships require properly correlating experimental data and theoretical studies. For example, recent studies from the Klapötke group have examined the properties of a series of nitrated aromatics for use as energetic materials.^{4,5} In their work, the Klapötke group used the data gathered from several crystal structures to validate and expand upon previously published models for assessing the energetic potential of the materials. Through balancing less favorable O···O and O···N interactions with favorable O···H interactions, improved design of material properties was accomplished. Furthermore, their work allowed for a corrected computational model that is useful for predicting additional functional compounds.

Aromatic esters comprise another class of functional groups that are fundamentally important in all fields of chemistry. Aromatic esters are elementary groups in synthesis, biquitous in pharmaceuticals, and in materials design. Concerning crystal engineering, esters have been shown to

influence long-range ordering through their ability to accept multiple hydrogen bonds at both oxygen moieties (i.e., the carbonyl and alkoxy oxygen) of the functional group. For instance, a recent work by Venkatesan et al. examined a series of functionalized molecules bearing aromatic esters. In their studies, subtle changes in the packing of crystalline solids were affected by tailoring the electronic properties of several ester groups on the molecules, allowing for distinct intermolecular interactions to form. These changes in the intermolecular interactions allowed for a measure of control with respect to the solid-state materials.

The analysis of crystal structures remains a vital and fundamental area of research. Analyzing so-called "classical" structural characteristics (e.g., bond distances, angles, and connectivity)¹¹ has been critical to the development of the modern understanding of solid-state materials. Concomitant with the advancement of modern computers, researchers interested in advancing a deeper understanding of crystal

Received: December 13, 2023 Revised: March 15, 2024 Accepted: March 18, 2024



Figure 1. Drawings of the seven compounds examined herein. Coloring is used to highlight the systematic variation in the ester chains.

structures have worked to develop newer methods of investigation typically revolving around the analysis of noncovalent interactions (NCIs). Several accessible and approachable programs now exist wherein crystal structures can be rigorously analyzed and their interactions carefully scrutinized. The references herein are solely based on the authors' experiences and do not in any way reflect the entirety of the available software. Despite the available software and the wealth of data they can produce, there remains the question of how crystals form and which, if any, interactions are more "important" in this process. 17

Herein, we present the synthesis, structural characterization, and computational study of a series of nitroaromatics bearing ester functional groups (Figure 1). The steric and electronic impacts of halogenated alkyl groups on the ester moiety are evaluated through systematically varying hydrogen for fluorine, chlorine, or bromine atoms. A combination of steric encumbrance and NCIs arising from the different functional moieties of the aromatic ring leads to the isolation of a set of conformational polymorphs. The impact of sterics is further probed by incorporating isopropyl, trifluoroisopropyl, and tertbutyl groups, leading to the formation of room-temperature liquids. Examining the solid-state structures helps to rationalize the formation of the liquid derivatives by clarifying the importance of π -stacking interactions to the formation of the extended structures. Furthermore, the liquid compounds are examined with variable-temperature viscosity and density studies, allowing us to derive mathematical models to rationalize the liquid-phase behavior of these compounds (see Supporting Information—Discussion).

2. MATERIALS AND METHODS

2.1. Chemicals. *2.1.1. Spectroscopy.* ¹H, ¹³C, and ¹⁹F NMR spectroscopy was performed on both JEOL 400 MHz NMR and Bruker 500 MHz NMR spectrometers. NMR solvents were purchased from Cambridge Isotope Laboratories. NMR shifts are referenced to the residual solvent peaks.

2.1.2. Thermal Properties. Melting points, glass transitions, and crystallization temperatures were measured using both a TA Discovery Q250 differential scanning calorimeter and a PerkinElmer 8000 differential scanning calorimeter. Each sample was placed in an aluminum pan and cycled three consecutive times from -50 to $100\,^{\circ}\text{C}$ at a heating and cooling rate of $10\,^{\circ}\text{C}/\text{min}$ with nitrogen purge gas. A 3 min isothermal step was included at the minimum and maximum temperatures of each cycle. Determined by the TRIOS analysis software, melting points were reported as the melting onset temperature, and glass-transition temperatures were reported as midpoints of phase transitions. Enthalpy values for the phase transitions were calculated using TRIOS software. All measurements were carried out under a nitrogen atmosphere (50 mL/min) and were reproducible to $\pm 1\,^{\circ}\text{C}$.

Variable-temperature viscosity and density data were acquired by using an Anton Paar SVM 3001 kinematic viscometer. Measurements were taken from 20 to 80 $^{\circ}$ C at increments of 5 $^{\circ}$ C.

2.1.3. Single-Crystal Diffraction. Single crystals for compounds 1 and 2 were coated in Cargille type A immersion oil and transferred to the goniometer of a Rigaku XtaLAB Mini diffractometer with Mo K α wavelength (λ = 0.70926 Å) and a CCD area detector. Examination and data collection were performed at 170 K. Data was collected, reflections were indexed and processed, and the files were scaled and corrected for absorption using CrysAlis Pro. ⁵⁴

Single crystals of compounds 3, 4-M, and 4-O were coated with Parabar 10312 oil and transferred to the goniometer of a Bruker D8 QUEST ECO diffractometer with Mo K α wavelength (λ = 0.71073 Å) and a photon II area detector. Examination and data collection were performed at temperatures as noted. Data was collected, reflections were indexed and processed, and the files were scaled and corrected for absorption using APEX3¹⁸ and SADABS.¹⁹

For all compounds, the space groups were assigned and the structures were solved by direct methods using XPREP within the SHELXTL suite of programs 20,21 and refined by full-matrix least-squares against F^2 with all reflections using Shelxl2018 22 using the graphical interface Olex2. 23 H atoms were positioned geometrically and constrained to ride on their parent atoms. C–H bond distances were constrained to 0.95 Å for aromatic and alkene C–H moieties and to 0.99 and 0.98 Å for aliphatic CH2 and CH3 moieties, respectively. Methyl H atoms were allowed to rotate, but not to tip, to best fit the experimental electron density. $U_{\rm iso}({\rm H})$ values were set to a multiple of $U_{\rm eq}({\rm C})$ with 1.5 for CH3 and 1.2 for C–H and CH2 units, respectively.

Complete crystallographic data, in CIF format, have been deposited with the Cambridge Crystallographic Data Centre. CCDC 2313816—2313820 contain the supplementary crystallographic data for this paper. These data can be obtained free of charge from The Cambridge Crystallographic Data Centre via www.ccdc.cam.ac.uk/data request/cif.

Hirshfeld surfaces, images, fingerprint plots, and frameworks were calculated and produced using CrystalExplorer21. ¹² Imaging and analysis of the structures were accomplished using Mercury ¹⁵ and Olex2.

VisualHabit²⁴ integrated within the Mercury suite of software²⁵ was used to calculate the attachment energy (AE) morphology of the compounds following established protocols.²⁶ Lattice energy calculations were accomplished with the Dreiding II²⁷ force field. The interaction energies calculated by CrystalExplorer and Mercury differ due to their method of calculation.²⁵ The relative magnitudes were used for discussion. That is, the calculated energies of the most stabilizing synthon in both methods were used to draw conclusions and make the rankings (and so on) rather than their specific values. The distances shown in the synthon images within the supplemental information are between molecular centroids.

CrystalGrower²⁸ in conjunction with ToposPro²⁹ was used to simulate the growth of **4-O** and **4-M**. The procedure we followed was outlined within the relevant literature. The relevant settings are provided in the Supporting Information, which details the input

Table 1. Compiled Physicochemical Data for Compounds 1-4

	molecular weight (g/mol)	crystalline void space, % of unit cell	Hirshfeld surface volume $(V_{\rm H}~{\rm \AA}^3)$	$\binom{T_{\mathrm{m}}}{(^{\circ}\mathrm{C})}$	$(^{\circ}C)$	$({}^{\circ}\overset{T_{g}}{C})$	lattice energy (kJ mol ⁻¹)	data collection temperature ^a (K)
1	195.17	35.4 ų, 3.8%	226.6	40.92			-71.2	170
2	249.14	72.5 Å ³ , 7.2%	248.2	46.65	-13.14		-98.7	170
3	298.50	44.8 ų, 7.8%	281.7	74.31	8.91	-42.20	-110.2	109
4-M	431.86	36.4 ų, 6.0%	291.7	83.83	33.07	-25.28	-118.1	100
4-O	431.86	74.6 ų, 6.1%	299.3				-119.0	150
^a Temperature of data collection for the crystallographic data.								

conditions for the simulation. A minimum omega value of 8 was used

for both 4-M and 4-O when calculating interactions for the simulations.

In brief, the interactions for both polymorphs were identified and tabulated, and the appropriate files were exported using ToposPro. Then the interactions were visually classified (e.g., π stacking, hydrogen bonding, etc.) in conjunction with VisualHabit within Mercury and given scaled values within the CrystalGrower software. These scaled values are, in part, determined by the interaction energies calculated in Mercury and CrystalExplorer. For example, in compound 4-O, interaction type A corresponds to a π stacking and was assigned a final scaled value of 5. The interaction scaling was systematically varied until a result was achieved that closely resembled the experimental morphology. Final scaling values are provided in the Supporting Information.

The simulated temperature of crystal growth was 25 $^{\circ}$ C and 2,000,000 iterations were used. Supersaturation profile 3 was used for all simulations, with a $\Delta\mu_1$ value of 100 kcal/mol.

OVITO³⁰ was used to visualize the results of the simulation and produce the final images and movies.

2.1.4. Computational Studies. All computations and resultant data were obtained using the Spartan software suite (Spartan'20, Wave function, Inc., Irvine, CA USA). The initial geometries from the crystal structures of compounds 1 and 4-M were loaded into the software and the geometry was optimized employing the M06-2X functional³¹ with the 6-311++G(2d,2p) basis set. Hydrogen distances were optimized, as well. A final single-point energy calculation was completed on the optimized models with the same functional and basis set. Vibrational frequencies were checked for imaginary values to ensure that the resultant structures were at a minimum.

A summary of the relevant thermophysical properties utilized in the analysis of the compounds is provided in Table 1.

3. EXPERIMENTAL SECTION

3.1. Synthesis. Synthesis of the compounds was accomplished following modified procedures from previous reports. 32,33 In brief, 3-nitrobenzoyl chloride (1 equiv), the appropriate alcohol (2 equiv), and pyridine (2 equiv) were dissolved in dichloromethane. The reaction flask was sealed, and the contents were magnetically stirred at room temperature overnight. In some cases, a white crystalline solid formed which was determined to be the hydrolyzed impurities. 34 The solid was filtered off, and the organic layer was washed with 0.5 M aqueous sodium bicarbonate solution (3 × 25 mL), followed by dilute 0.1 M hydrochloric acid washes (3 × 25 mL), and finally brine. The solvent was removed under reduced pressure, and the resulting compounds were purified by column chromatography (9:1 DCM/MeOH mobile phase, silica gel stationary phase) yielding the desired final products.

3.1.1. Ethyl m-Nitrobenzoate (1). Clear oil solidified upon cooling to room temperature. Yield: 65%.

Single crystals suitable for diffraction formed upon cooling to room temperature.

¹H NMR (400 MHz; CDCl₃): δ 8.84 (t, J = 1.8 Hz, 1H), 8.41–8.35 (m, 2H), 7.64 (t, J = 8.0 Hz, 1H), 4.43 (q, J = 7.1 Hz, 2H), 1.42 (t, J = 7.1 Hz, 3H).

(t, J = 7.1 Hz, 3H). 13 C NMR (75 MHz; CDCl₃): δ 164.62 (s, 1C), 148.44 (s, 1C), 148.42 (s, 1C), 135.41 (s, 1C), 132.39 (s, 1C), 129.71 (s, 1C), 127.43 (s, 1C), 124.70 (s, 1C), 62.09 (s, 1C), 14.42 (s, 1C). 3.1.2. 2,2,2-Trifluoroethyl m-Nitrobenzoate (2). Pale yellow oil, which solidified upon cooling to room temperature. Yield: 72%.

Single crystals suitable for diffraction formed upon cooling to room temperature.

¹H NMR (400 MHz; CDCl₃): δ 8.89 (t, J = 1.9 Hz, 1H), 8.49–8.39 (m, 2H), 7.72 (t, J = 8.0 Hz, 1H), 4.77 (q, J = 8.3 Hz, 2H).

 ^{13}C NMR (75 MHz; CDCl₃): δ 163.11 (s, 1C), 135.70 (s, 1C), 130.28 (s, 1C), 130.14 (s, 1C), 128.46 (s, 1C), 125.16 (s, 1C), 61.74 (s, 1C), 61.26 (s, 1C), 31.08 (s, 1C).

¹⁹F NMR (376 MHz; CDCl₃): δ –73.49 (t, J = 7.7 Hz, 3F).

3.1.3. 2,2,2-Trichloroethyl m-Nitrobenzoate (3). White solid. Yield: 72%.

Single crystals suitable for diffraction were grown from the slow evaporation of dichloromethane.

¹H NMR (400 MHz; CDCl₃): δ 8.93 (t, J = 1.8 Hz, 1H), 8.49–8.44 (m, 2H), 7.73 (t, J = 8.0 Hz, 1H), 5.03 (s, 2H).

¹³C NMR (75 MHz; CDCl₃): δ 162.92 (s, 1C), 148.45 (s, 1C), 135.58 (s, 1C), 130.48 (s, 1C), 129.98 (s, 1C), 128.24 (s, 1C), 125.05 (s, 1C), 94.54 (s, 1C), 74.80 (s, 1C).

3.1.4. 2,2,2-Tribromoethyl m-Nitrobenzoate (4). White solid. Yield: 78%.

Single crystals of the monoclinic polymorph were taken from a batch of crystals grown from the slow evaporation of acetone. Crystals of the orthorhombic polymorph were found in a batch of crystals grown from the slow evaporation of dichloromethane.

¹H NMR (400 MHz; CDCl₃): δ 8.98 (t, *J* = 1.9 Hz, 1H), 8.50–8.48 (m, 2H), 7.73 (t, *J* = 8.0 Hz, 1H), 5.21 (s, 2H).

 $^{13}\mathrm{C}$ NMR (75 MHz; CDCl₃): δ 162.86 (s, 1C), 148.62 (s, 1C), 135.75 (s, 1C), 130.80 (s, 1C), 130.14 (s, 1C), 128.35 (s, 1C), 125.24 (s, 1C), 77.74 (s, 1C), 34.92 (s, 1C).

3.1.5. Isopropyl m-Nitrobenzoate (5). Clear liquid. Yield: 64%.

¹H NMR (400 MHz; CDCl₃): δ 8.74 (t, J = 1.9 Hz, 1H), 8.33–8.28 (m, 2H), 7.60 (d, J = 16.0 Hz, 1H), 5.23 (7, J = 6.3 Hz, 1H), 1.34 (d, J = 6.4 Hz, 6H).

¹³C NMR (75 MHz; CDCl₃): δ 164.11 (s, 1C), 135.42 (s, 1C), 132.80 (s, 1C), 129.65 (s, 1C), 127.34 (s, 1C), 124.65 (s, 1C), 69.87 (s, 1C), 31.08 (s, 1C), 22.04 (s, 1C).

3.1.6. tert-Butyl m-Nitrobenzoate (6). Pale yellow liquid. Yield: 46%.

¹H NMR (400 MHz; CDCl₃): δ 8.70 (t, J = 1.9 Hz, 1H), 8.31 (ddd, J = 8.2, 2.3, 1.1 Hz, 1H), 8.25 (dt, J = 7.8, 1.2 Hz, 1H), 7.58 (t, J = 8.0 Hz, 1H), 1.56 (s, 9H).

¹³C NMR (101 MHz; CDCl₃): δ 163.47 (s, 1C), 148.14 (s, 1C), 135.18 (s, 1C), 133.70 (s, 1C), 129.45 (s, 1C), 126.91 (s, 1C), 124.35 (s, 1C), 82.56 (s, 1C), 28.07 (s, 3C).

3.1.7. 2,2,2-Trifluoro-1-(trifluoromethyl)ethyl m-Nitrobenzoate (7). Pale yellow liquid. Yield: 60%.

¹H NMR (400 MHz; CDCl₃): δ 8.89 (t, J = 2.0 Hz, 1H), 8.54–8.43 (m, 2H), 7.78 (t, J = 8.0 Hz, 1H), 6.09–6.00 (m, 1H).

¹³C NMR (75 MHz; CDCl₃): δ 161.65 (s, 1C), 148.67 (s, 1C), 136.00 (s, 1C), 130.47 (s, 1C), 129.28 (s, 1C), 128.72 (s, 1C), 125.57 (s, 1C), 67.43 (dq, J = 69.3, 34.2 Hz, 1C), 31.07 (s, 1C).

¹⁹F NMR (376 MHz; CDCl₃): δ -73.32 (d, J = 5.8 Hz, 6F).

4. RESULTS AND DISCUSSION

4.1. Molecular Structure Analysis. Compounds 1–4 were crystallized and their structures were examined via single-

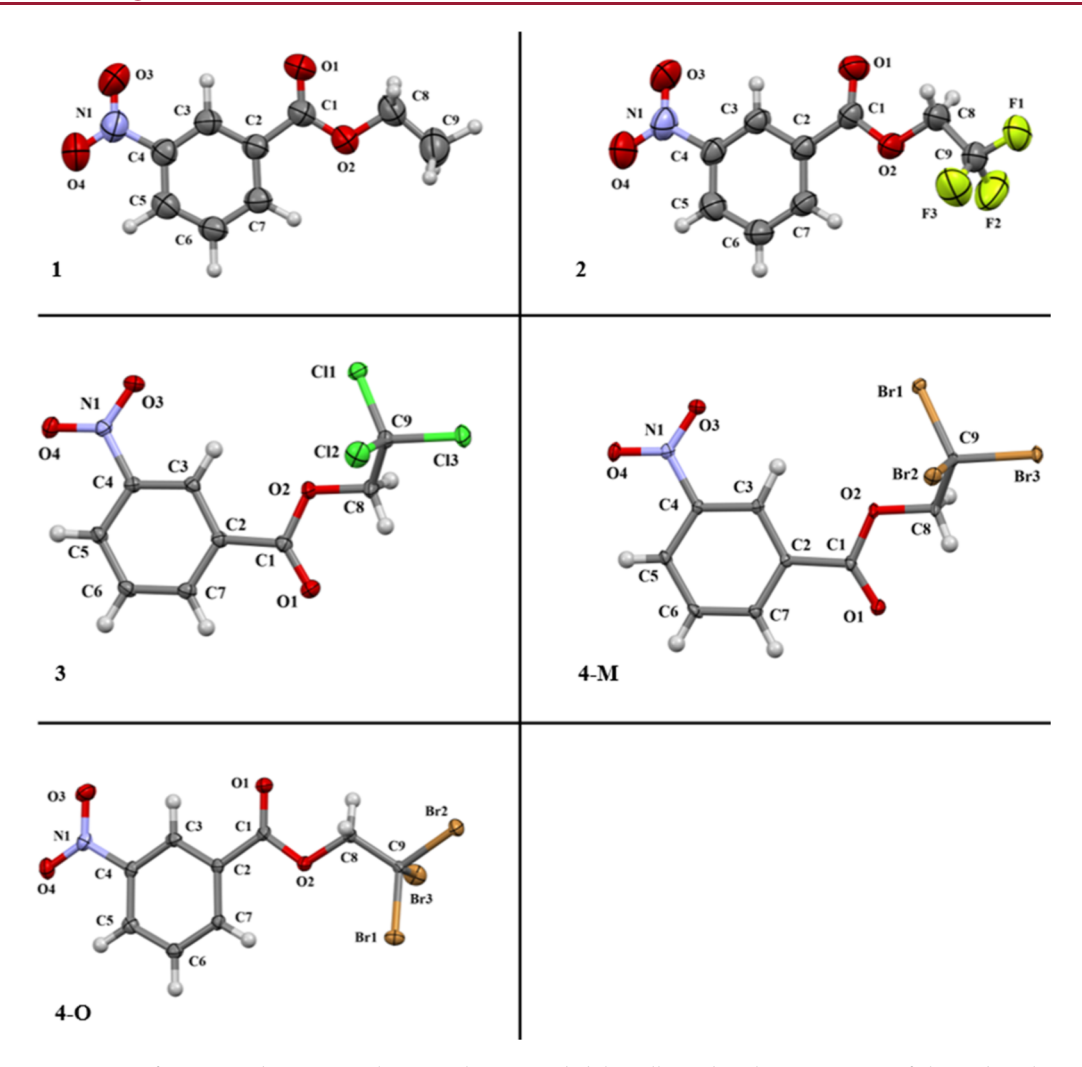


Figure 2. Asymmetric units of compounds 1-4 are shown with 50% probability ellipsoids. The orientation of the carbonyl oxygen (O1) with respect to the rest of the molecule is an important distinction in the conformational polymorphs. Gray = carbon; blue = nitrogen; red = oxygen; yellow = fluorine; green = chlorine; tan = bromine.

crystal X-ray diffraction. Compound 4 crystallizes in two unique conformational polymorphs^{3.5} which will be referred to as **4-M** and **4-O** for the monoclinic and orthorhombic forms in which they crystallize. Structures **1**, **2**, and **3** also crystallize in the monoclinic crystal system. **1** crystallizes in the $P2_1/c$ space group, **2** in $P2_1/n$, both **3** and **4-M** in $P2_1$, and **4-O** in $P2_12_12_1$. All five of the structures have only one molecule in the asymmetric unit with no observed disorder (Figure 2).

Two key points of distinction should be addressed, with respect to the overall geometries of the molecular structures. First is the overall orientation of the carbonyl group. Structures 1, 2, and 4-O have similar molecular geometries, wherein the orientation of the carbonyl oxygen of the ester aligns with the C3–H moiety on the aromatic ring. Compounds 3 and 4-M, however, have a different orientation with the carbonyl oxygen being oriented at 120° from that seen in 1 and 2. Figure 3 provides clarity with respect to the orientation of the carbonyl groups.

Second is the torsion angle in the alkyl chains. In 1 and 2, the ester alkyl chain carbon atoms are nearly coplanar with the carbonyl moiety, having a C1-O2-C8-C9 torsion angle of approximately 175° . This same angle for 3 and 4-M and 4-O is approximately 150° . The inclusion of the sterically demanding trichloromethyl and tribromomethyl groups appears to

$$O_2N$$
 H_3
 O_2N
 H_5
 O_2N
 H_5
 O_2N
 O_3
 O_2N
 O_3
 O_4
 O_5
 O_5

Figure 3. Depictions of the two orientations of the carbonyl groups observed in the compounds. Aromatic hydrogens H3 and H5 are shown for the sake of clarity.

influence the torsion angle of the ethyl chain on the ester moiety, showing a preference for the 150° orientation. Thus, the combination of the carbonyl orientation along with the torsion angles on the alkyl group effectively makes for two distinct sets of conformations with respect to the overall molecular structure.

4.2. Surface Analysis and Interactions. To evaluate the structural impacts brought about by the varying compositions and molecular geometries, Hirshfeld surface analysis was performed on all five structures and their fingerprints were analyzed for prominent structural features.³⁶ Hirshfeld surface analysis allows for quantifications of the interactions from individual atom contacts, the values of which are provided in

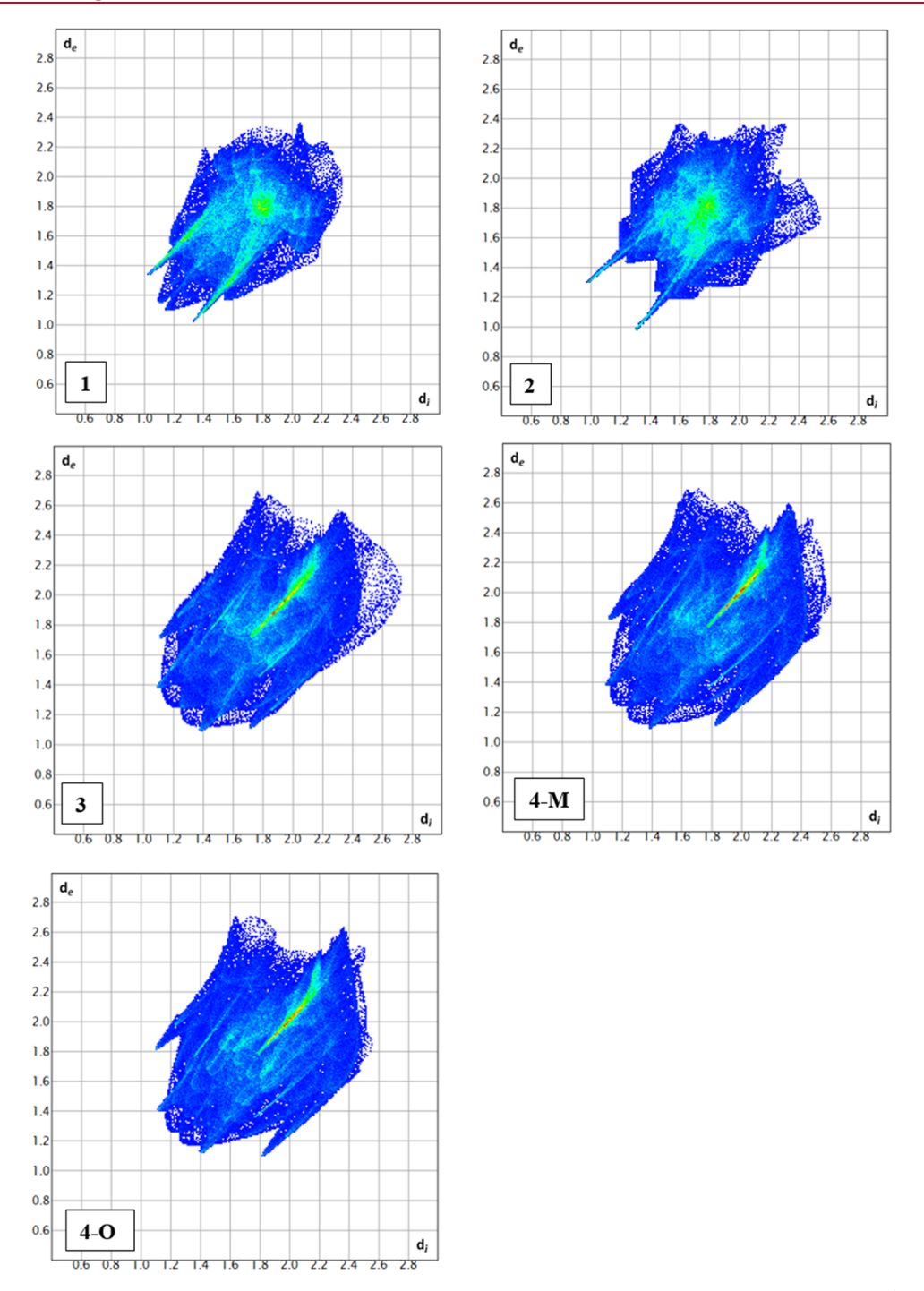


Figure 4. Complete interaction fingerprints for compounds 1–4-O. Important interactions, such as hydrogen interactions (spikes) and halogen contacts (red regions), are observed within the compounds.

the Supporting Information. The complete fingerprints for the structures are listed in Figure 4.

As expected, given the general similarity of the structures, the fingerprints for the five compounds share common features. First, all compounds display characteristic spikes arising from hydrogen interactions. Specifically, these spikes arise from reciprocal H···OlO···H interactions originating from nitro and carbonyl oxygen moieties. Second, a distinct red region is noted for compounds 3, 4-M, and 4-O. This feature is a consequence of halogen···halogen interactions. While F···F interactions are present in 2, these do not manifest in a similar way on the fingerprints. Finally, each fingerprint displays a

region of dispersed interactions at the higher $d_{\rm i}/d_{\rm e}$ ranges. These are attributed to inefficient packing within the crystal (see Supporting Information—Discussion).³⁷

Compounds 4-M and 4-O are polymorphs, allowing for direct comparisons of the distinct conformations of the ester group and how the different orientations can change interactions. Examining the numerical percentage of the interactions provided reveals some key observations (see Supporting Information—Interactions and Synthons). First, in both crystals, the highest percentage of interactions is of the Br···Br contacts. The two structures have nearly identical percentages of Br···Br contacts (20.8 vs 20.5%). Second, 4-M

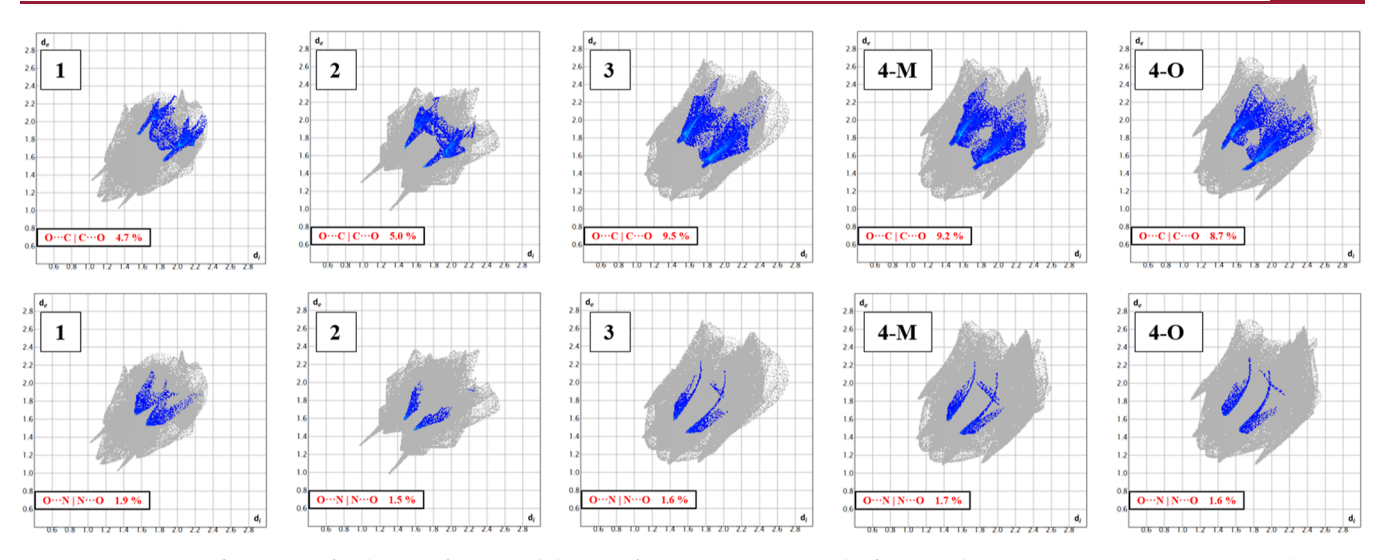


Figure 5. Interaction fingerprints for the O···ClC···O and the O···NlN···O interactions in the five crystal structures. Unique interaction synthons are observed upon comparison of the blue regions within compounds 1 to 2. Similarities in the interactions are observed in compounds 3, 4-M, and 4-O.

has a slightly higher percentage of H···H interactions (12.4 vs 11.0%) while **4-O** has a marginally higher percentage of H···O interactions (11.5 vs 12.1%), though the numerical differences are rather small in all cases.

Looking at these interactions reveals that, overall, the differences in these Br and H interactions for the polymorphs appear minor at best (see Supporting Information—Images S1). For example, in both compounds, two of the bromine atoms are predominantly involved in Br···Br interactions. The geometric similarity of the interactions, with respect to both distances and angles, is thus reflected by the comparable numerical percentages calculated in the Hirshfeld analysis. Therefore, we set about to complete a more rigorous examination of the polymorphs to help deduce how specific interactions influence the formation of the crystal structures. To accomplish this, a systematic analysis of the interactions is necessary.

4.2.1. Hydrogen Interactions. All of the compounds have a comparable set of individual interaction percentages, with the interactions involving hydrogen accounting for a large percentage of the total interactions. This is most prevalent in 1, wherein over 50% of the intermolecular interactions involve hydrogen. As the methyl hydrogen atoms in 1 are substituted for halogens, the relative percentage of interactions involving hydrogen decreases, as expected.

Contrasting the hydrogen interaction motifs in the five crystals reveals several noteworthy structural principles. All five of the compounds display $H\cdots O_{NO_2}$ interactions with these interactions typically being the shortest of the hydrogen interactions. For example, 1 has the shortest $H\cdots O_{NO_2}$ distance at 2.37 Å $\{d[HS^i\cdots O3, \angle N1-O3\cdots HS^i=131.3(5)^\circ, i=-x, 1/2+y, 1/2-z]\}$. Within this set of compounds, the nitro moiety displays four distinct hydrogen interaction motifs. Specifically, 1, 2, and 4-O all display unique hydrogen interaction synthons, while 3 and 4-M display virtually identical synthons. The similarities, and differences, of these interactions are readily observable when examining the H interaction fingerprints derived from Hirshfeld surface analysis (see Supporting Information—Images S2–S4).

As a consequence of the varied geometry of the H-interactions, it can be concluded that while these $H\cdots O_{\rm NO_2}$ are important to the overall formation of the crystals, these are likely not the principal synthons leading the crystal formation for these compounds. This observation helps, in part, to rationalize the formation of polymorphs, given the varying options in which these H interactions could form. That is, if there are multiple H interaction synthons which are energetically accessible and are reasonably similar in stabilization energy, then there are multiple ways in which the solid-state structures may form. 39

4.2.2. Oxygen Interactions. Unique features in the fingerprints point to distinctive sets of interactions in the solid state arising from both the nitro and carbonyl oxygen moieties. All five compounds exhibit a region of reciprocal O··· C/NIN/C···O interactions, wherein oxygen atoms from carbonyl and/or nitro moieties interact with π bonds (Figure 5). These O··· π interactions appear at the green regions in the fingerprints near the central portion of the shape. As discussed for the H interactions, there are distinctive interaction motifs arising from the oxygen atoms. For example, 3 and 4-M have nearly identical shapes and percentages and therefore display nearly identical C···OlO···C interactions (see Supporting Information—Discussion).

While 1 and 2 both display side-on stacking interactions when examining the nitro and carbonyl oxygens, the interactions are distinct. For 1, the arrangement is such that one oxygen of the nitro group is interacting in a vertical manner with the π hole of a symmetry adjacent nitro group, thus accounting for both interactions (i.e., C and N). Compound 2, however, displays a vertical stacking interaction arising from reciprocal O···C/NIC/N···O interactions involving both the nitro and carbonyl moieties. Thus, 1 and 2 show two unique stacking interactions of the oxygen-containing moieties in the molecule despite having comparable percentages of O···C/NIC/N···O interactions.

Compound 3 and both polymorphs of 4 show nearly identical arrangements, wherein both end-on and side-on interactions of the nitro moieties are observed, forming the third $O\cdots C/N|C/N\cdots O$ motif. In all three of the compounds (3, 4-M, and 4-O), both the O_{NO} , and the O_{CO} moieties are

 Crystal Growth & Design
 pubs.acs.org/crystal
 Article

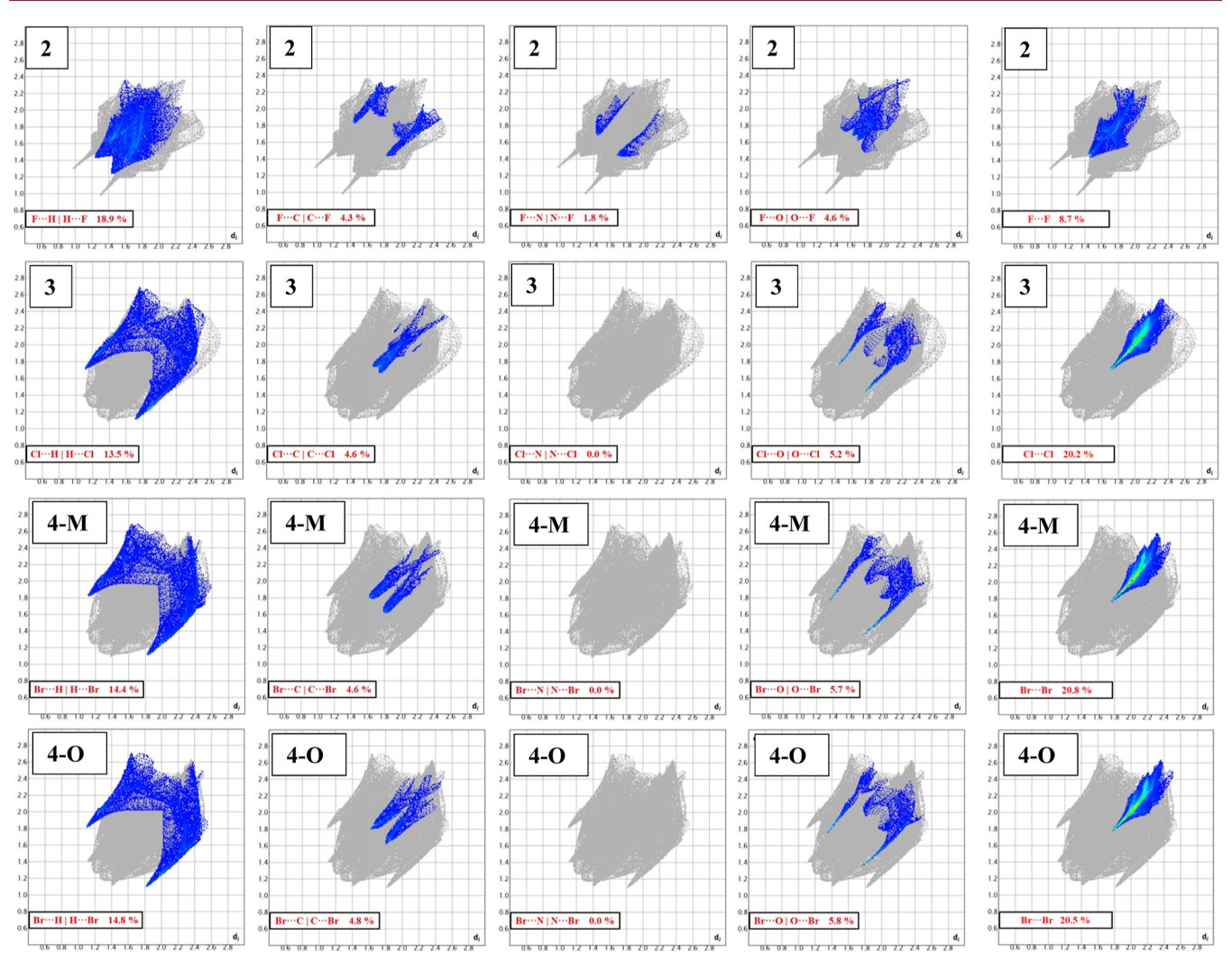


Figure 6. Interaction fingerprints of the halogen interactions for compounds 2–4-O. Compounds 3, 4-M, and 4-O display similar interactions and percentages as shown by the similar shapes in the fingerprints.

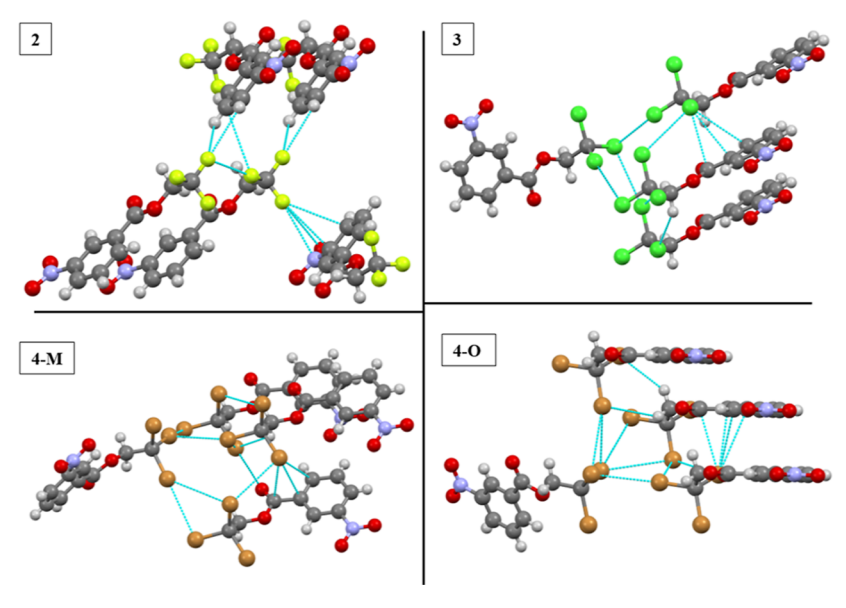


Figure 7. Depiction of the halogen interactions in the compounds ($X \cdots H$, C, and N). Maximum interactions were set to van der Waals radii of the atoms +0.3 Å.

seen interacting with adjacent π bonds on the aromatic ring in a side-on manner. Numerous interactions exist between the nitro moiety and carbons on the aromatic ring (π bonds) in addition to interactions with the carbonyl carbon ranging in distance from 3.12 to 3.48 Å.

4.2.3. Halogen Interactions. Figures 6 and 7 show the fingerprints and a depiction of the halogen interactions for 2—4-M and 4-O. All four of the halogen-containing crystals show domains wherein the arrangement of the molecule leads to the formation of halogen···halogen contacts at similar distances and angles as observed in previous reports. 40—42 These regions of halogen interactions typically manifest in the central portion of the fingerprint plots and are most evident in 3, 4-O, and 4-M with bright green and red "lines".

Indeed, several of the halogen···halogen interactions in 3, 4-M, and 4-O do fall on the shorter end of reported distances. 43-46 For example, 3 exhibits a number of Cl···Cl contacts, with the shortest being 3.4356(4) Å (Cl3···Cl3 j , j =-x, 1/22 + y, 2 - z). For 4-M, Br3 displays interactions with symmetry adjacent to Br2 and Br3 atoms. Specifically, Br3... Br3^k (k = -x, -1/2 + y, 2 - z) is at a distance of 3.5503(5) Å with 156.78(9) and 95.14(8)° angles (\angle C9-Br3^k···Br3, \angle C9-Br3···Br3^k). It should be noted that while compounds 3 and 4-M and O do exhibit close halogen...halogen interactions, the angles and distances involved appear just outside the established ranges indicative of type I or II halogen bonds. 47-49 However, these contacts are certainly significant in the formation of the crystal morphology given the high percentage of Cl···Cl and Br···Br interactions observed (see Section 4.4).

Structures 3, 4-M, and 4-O show interactions wherein the carbonyl oxygen (O1) is interacting with a halogen on a symmetry adjacent molecule, forming a σ -hole interaction (Figure 8). Contrasting the polymorphs 4-M and 4-O, the O1···Br1 distances of 3.132(3) and 3.147(2) Å, respectively, are less than the sum of van der Waals radii of the individual atoms. The C1-O1···Br1 angles in 4-M and 4-O are 174.8(8) and 170.37(10)°. For 3, the related distance and angle are 3.2283(11) Å and 171.8(1)°. These halogen bonds help to form the planar arrangement of the molecules. Of note is that both orientations of the carbonyl group (see Figure 3) maintain these O···X interactions. This lends evidence to the noncircumstantial nature of these chalcogen bonds. 53,55,56

To summarize, several key details emerge when examining the halogen interactions with the crystals. First, both σ - and π -hole interactions are present. Specifically, we observe $O_{CO}\cdots$ Cl/Br interactions in 3 and 4 while in 2, F···O $_{NO_2}$ are seen (see Supporting Information—Discussion). Second, halogen···halogen interactions comprise a significant portion of the total interaction percentages for compounds 2–4. Finally, the change in ester orientation does not appear to have any notable impact on the interactions in 4-M vs 4-O. Both orientations maintain the $O_{CO}\cdots X$ chalcogen bonds.

4.3. Energy Frameworks and Interaction Synthons. Energy frameworks offer insights into the packing and growth of the crystalline state of the compounds. A representative framework for compounds 1–4-O is shown in Figure 9. A complete view of the frameworks is provided in the Supporting Information along with tables listing the interaction energies. The width of the colored columns in the images corresponds to the relative magnitude of the interaction energy along that

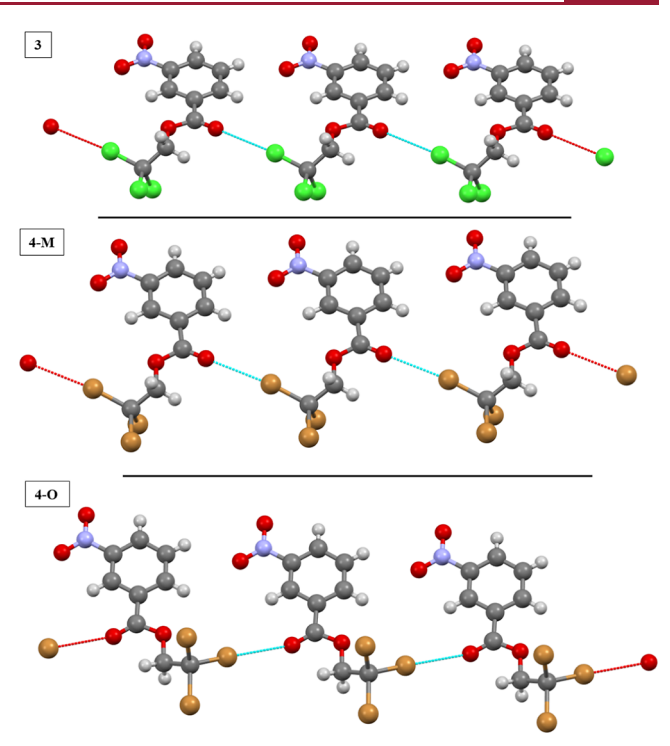


Figure 8. Depiction of the carbonyl···halogen σ -hole interactions forming the planar arrangement of compounds **3**, **4-M**, and **4-O**. Red dotted lines indicate the continuation of the interactions.

direction and the coloring corresponds to the dispersion (green), Coulombic (red), and total energy (blue). 57

Examining the calculated frameworks reveals key details about the compounds. First, and most importantly, for all compounds examined, the interactions with the highest stabilization energy (most negative value) arise from stacking interactions. This is made clear by the larger cylinders in the frameworks connecting the distinct layers of the molecules. As an example, in 1, the interactions with the highest stabilization correspond to the purple and green molecules. These are both stacking interactions, wherein the interactions arise between the aromatic π system and adjacent ketones and nitro moieties. It should be noted that these stacking interactions are more complex than just simple aromatic π – π stacking. For example, in 3, in addition to the π - π interactions, the stacking synthons also involve Cl···Cl and H···Cl contacts. Thus, these stacking synthons themselves represent a complex set of interactions to interpret beyond simply discussing atom-atom contacts.

As follows from the previous discussions, compounds 3 and 4-M show strong similarities with regard to frameworks. The Coulombic frameworks for 3 and 4-M are nearly identical in magnitude and directionality, though some notable trends are observed. The strongest interactions in 3 arise from two stacking interactions as described above (green, $E_{\text{tot}} = -26.7 \text{ kJ}$ mol^{-1} ; yellow, $E_{\text{tot}} = -24.6 \text{ kJ mol}^{-1}$). Surprisingly, the observed σ -hole interactions are not as stabilizing as these π interactions, though they are significant ($E_{\rm tot}$ = -18.1 kJ mol⁻¹). Finally, the two sets of Cl···Cl interactions are only weakly stabilizing at best with $E_{\text{tot}} = -2.8 \text{ kJ mol}^{-1}$ and $E_{\text{tot}} =$ -4.6 kJ mol⁻¹. These trends follow closely with what is observed in 4-M. Of note, the energy of the O_{CO}···Br interaction in 4-M ($E_{\text{tot}} = -21.2 \text{ kJ mol}^{-1}$) is lower than that of the O_{CO} ···Cl ($E_{tot} = -18.1 \text{ kJ mol}^{-1}$) interaction in 3 following the trends for σ -hole interactions.

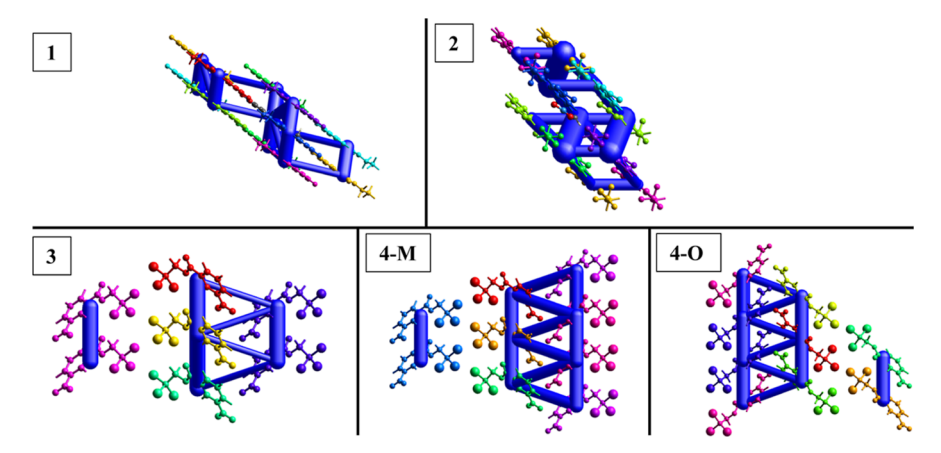


Figure 9. Total energy frameworks of compounds 1–4-O. Coloring of molecules shown for clarity. 1 and 2 are viewed down the crystallographic B axis. 3, 4-M, and 4-O are viewed down the crystallographic A axis.

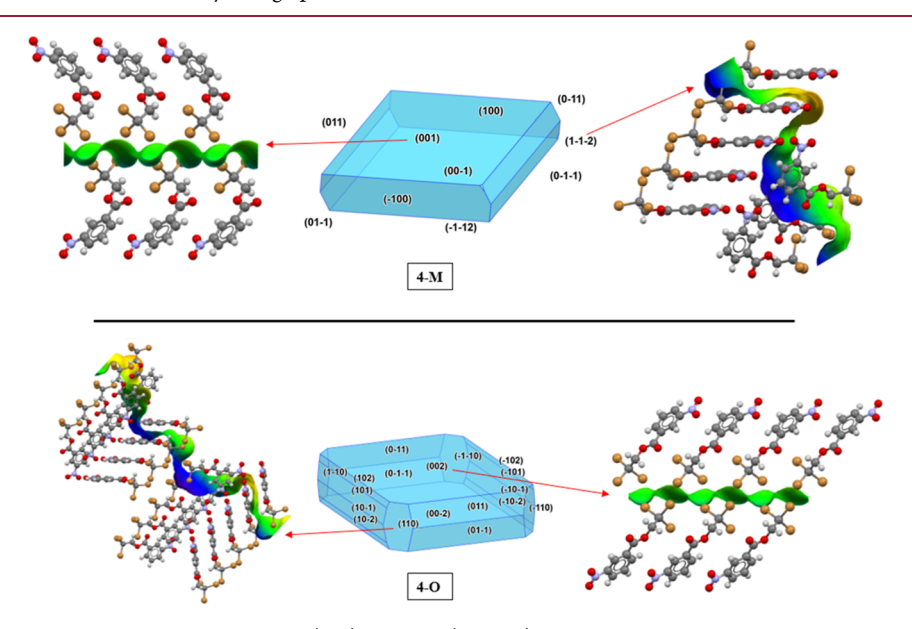


Figure 10. Predicted morphology of the crystals of 4M (top) and 4O (bottom). The surfaces with the highest and lowest AEs are shown.

ī

The polymorphs (4-M and 4-O) offer a chance to examine some of the rationale behind the formation of the two crystalline solids. Both frameworks for the structures are overall very similar, following with the discussion of the interactions. A point of distinction is the O_{CO}···Br interaction wherein 4-M has modestly stronger interactions than 4-O at -21.2 vs -19.7kJ mol⁻¹, respectively. The O_{CO}···Br distances of the two interactions are comparable at 3.146(2) Å for 4-M and 3.132(3) Å for 4-O $d(O \cdot \cdot \cdot Br)$. The distinction thus seems to be with the angle of the interactions wherein 4-M is more linear at $165.7(2)^{\circ}$ vs **4-O** at $161.1(3)^{\circ}$ ($\angle C1-O1\cdots Br1$). However, it should be noted that this difference in energy is rather small when considering the interactions present throughout the entire crystal. Thus, it would be incorrect to assume that this specific difference is a driving force for polymorph formation, particularly when the influence of solvents and ambient thermal energy is considered.

In summary, a number of notable observations from the energy frameworks lead to a more complete understanding of the crystal structures and interactions present in these molecules. First, for all the samples examined, stacking interactions with the aromatic system (e.g., $\pi - \pi$, NO₂··· π , etc.) display the highest stabilization to the crystals. While the

exact nature and geometry of these interactions are different for each structure, the calculated synthons show similarities. Second, the face-on halogen···halogen interactions are only moderately stabilizing, in the range of -6 kJ mol⁻¹. Thus, these interactions seem to be a consequence of packing favoring other, more stabilizing interactions. Finally, the O_{CO} ···Br/Cl interactions follow the expected trends for σ -hole interactions, with interactions with bromine being of lower energy than the chlorine interactions.

4.4. Simulated Crystal Growth of 4-M and 4-O. Even within the relatively simple structures presented herein, a complex set of interaction synthons is responsible for the formation and subsequent growth of the crystals. Several methods exist to predict the morphology and growth of crystals that involve the use of the interactions derived from the molecular structure. The sequential changes from CH_3 to CBr_3 , and in particular the polymorphs of 4, present an excellent opportunity to study the theoretical impacts of how the differing geometry and composition impact the morphology of the crystals.

The calculated AE model morphologies of 4-M and 4-O are shown in Figure 10. Comparing the calculated morphologies of the crystals reveals similarities between the two compounds.

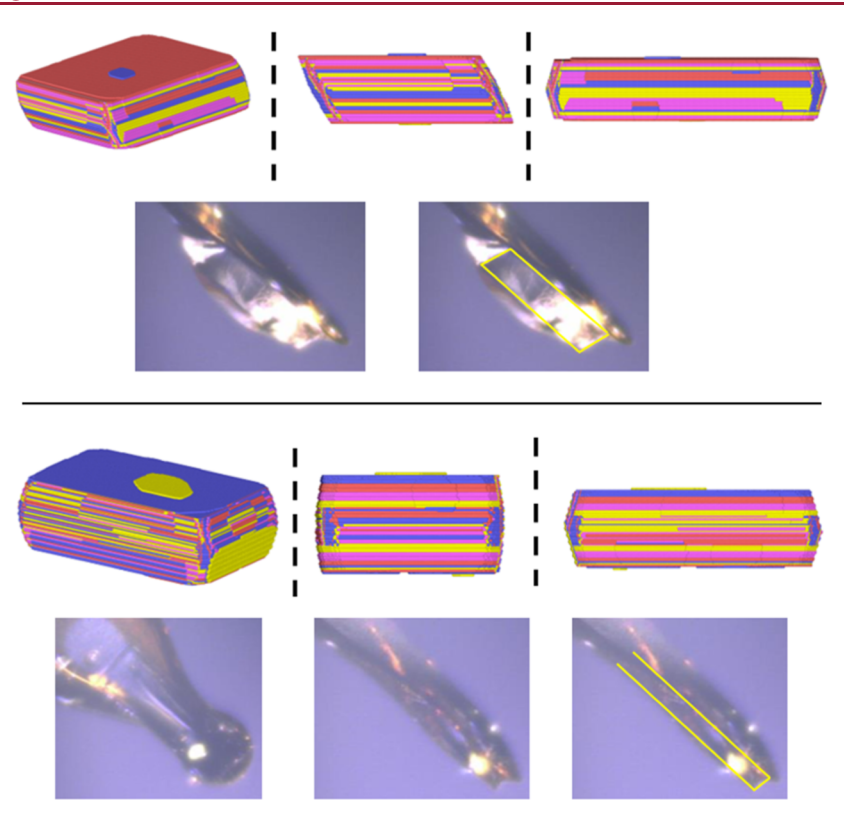


Figure 11. Simulated crystals of 4-M (top) and 4-O (bottom). Different angles are shown to provide a better view of the morphology. Images of the actual crystals are provided for comparison from different angles. Yellow outlines are shown to help clarify the morphology of the actual crystals.

Specifically, the calculated shapes of both appear as flat, plate-like crystals. Furthermore, the dominant faces in both cases are related, with the (001) face being dominant in 4-M and the (002) face being dominant in 4-O. Additionally, both morphologies share a similar overall shape with tapered edges composed of, predominantly, the (011), (01 $\overline{1}$), (0 $\overline{1}$ 1), and (0 $\overline{1}$ $\overline{1}$) faces.

Examining the surfaces and AEs⁵⁹ of 4-M and 4-O helps to verify the assessments made with respect to the interactions and frameworks' discussions (Section 4.3). A complete listing of the calculated surfaces and their respective energies for both polymorphs is provided in the Supporting Information. As has been established, 60 the surfaces with the smallest AEs, -16.3 kJ mol^{-1} for 4-M and -18.2 kJ mol^{-1} for 4-O, correspond to the largest faces of the crystals (by area). Figure 10 visualizes the surfaces of 4-M and 4-O. In both cases, these faces grow due to "face-on" Br...Br interactions. The small AE reinforces our previous assertion that these Br...Br interactions are not strongly stabilizing and, thus, likely are not classical halogen bonds. The surfaces with the largest AE for both crystals arise, in part, from the aforementioned stacking motifs. Thus, for the conformers, it is predicted that these stacking interactions are important to the growth of the crystal.

With our combined understanding of the interactions, synthons, and AEs of these compounds, we set about to experimentally validate the importance of specific interactions for the growth of these crystals. The CrystalGrower software allows for facile visualization of the growth of a crystal when providing information about interactions within the unit cell. For the immediate purposes of this paper, the software provides a way to close the loop, as it were, with respect to evaluating the importance of the interactions discussed. In brief, the process of setting up the simulation involves ascribing

scaled energies to different synthons within the unit cell leading to the growth of the extended structure.²⁸ Thus, several calculations were run in which the relative energies of the interactions were tuned until the simulated crystal shape matched the actual crystals as closely as possible.

The results from simulated crystal growth are shown in Figure 11. For both 4-M and 4-O, the simulated Crystal-Grower models (CG models) bear a strong resemblance to the AE models. For example, both models show the formation of plate-like crystals with a slow-growing (001) face. Furthermore, the sides of the CG models show the formation of the angled faces observed in both of the AE models discussed. However, we do see a key difference when contrasting the CG model for 4-M vs 4-O. Specifically, a more pronounced parallelogram-like morphology is observed for 4-M. 4-O, however, appears to form a morphology with rounded edges. Encouragingly, the actual crystals closely match these simulations, with the 4-M sample shown in Figure 11 having a slanted face. For 4-O, however, the crystal edges appear flat, with no readily observable rounded faces. However, the overall predicted morphology of flat, plate-like crystals matched well with the experimental samples.

For both of the CG models, the stacking interactions were key in the formation of the simulated crystals matching the experimental morphologies. Lowering the scaling for these interactions leads to the growth of crystals that neither match the actual morphologies nor the AE models, forming different morphologies not observed in the experimental crystals. Thus, the π interactions appear to be the controlling factor in the growth of the crystals, while the halogen interactions are less defining, relatively speaking, indicative of their secondary factor in the formation of the long-range order for the compounds.

Both the σ -hole and interactions involving the nitro group appear to play equally important roles with respect to the simulations. In both cases, equal scaling was given to these interactions, thus leading to the final morphologies presented. With respect to the σ -hole interactions, the directional nature of these interactions helps to form layers, which are also characterized by the presence of the O_{NO_2} ···H interactions. The lowest scaling was given to the interhalogen interactions, visualized as the faces with the lowest AEs for both compounds (Figure 10).

The additional conclusion is that a complex set of interactions is responsible for the formation of the solid state for these sets of compounds. Completely removing or significantly lowering scaling of the halogen-based interactions or the hydrogen interactions did not yield reasonable results. Thus, a balance of all of the interactions discussed herein leads to the observed crystal formation. However, with the simulated data, we were able to reasonably conclude that the π interactions appear more strongly stabilizing than the other interactions.

5. CONCLUSIONS

The formation of the crystalline solid state is complex. NCIs are the key components which hold molecular crystals together, forming the extended structures. Often, however, human "bias" can play a role in the interpretation of crystalline solids wherein statements are made about the importance of a singular interaction with respect to its role in stabilizing the crystal lattice. Herein our goal is to develop a workflow for understanding the physicochemical properties of a series of nitrated aromatic compounds. Our methodology is aided using modern crystallographic software which facilitates the understanding of the crystal structure of organic compounds, helping to assess the relative importance of specific interaction synthons (i.e., NCIs) within these systems.

In this work, we have been able to determine several key ideas and theories by studying this series of compounds:

- i. Simulated growth of crystals helps to reveal the relative importance of the π-stacking interactions in the formation of the crystals for these compounds. Similarities in the theoretical morphologies and the actual morphologies are noted for both 4-M and 4-O, such as the formation of thin plates with tapered edges. It should be stated, however, that the effect of solvent on the formation of the crystals is an area which would need to be investigated.
- ii. σ -hole interactions play a key role in the directional packing of the crystal. Specifically, carbonyl oxygen··· halogen interactions help form the planar arrangement of the molecules in either conformation observed with the ester. These σ -hole interactions are not observed with the fluorine-containing derivative, however.
- iii. The nitro moiety displays numerous distinct interactions involving the carbonyl and aromatic π moieties. Cursory examination of interactions may lead to the conclusion that O···O interactions arising from these functional groups are destabilizing. However, careful attention should be paid to the exact geometry of these interactions. For example, in compounds 3, 4-M, and 4-O, these O_{NO_2} interactions are a consequence of the oxygen atoms interacting with the π hole of the nitro moiety and are thus a stabilizing interaction. In 1,

however, the O_{NO_2} atoms are directly interacting with the O_{NO_2} atoms of symmetry adjacent molecules, likely a consequence of the careful balancing act a molecule must allow for more favorable interactions to be optimized.

- iv. F...F interactions appear to be disfavored over more stabilizing hydrogen-based interactions. This is observed in the decrease in packing efficiency of 2 vs 1. For this series of compounds, interactions are tailored, in part, by the orientation of the ester and alkyl moiety.
- v. Increasing the steric bulk of the compound via modification of the ester moiety leads to the formation of room-temperature liquids (i.e., compounds 5–7) speculatively by preventing the optimal long-range formation of the aforementioned stacking interactions (see Supporting Information—Discussion). Preliminary thermal analysis helps point to this conclusion by showing the expected increases in activation energy with increasing molecular weight. Further analysis of this theory, however, is warranted to draw definitive conclusions about the relationship between steric bulk and the formation of the liquids.
- vi. One point which certainly bears further scrutiny is the role of solvents in the formation of the polymorphs and the overall morphology of the crystals. Multiple crystal samples grown from different solvents were screened for compound 4. Most of those samples showed the monoclinic unit cell (i.e., 4-M), and data collection did not progress past a routine screening. The results of the simulation point toward the impact of solvents. For example, carbonyl-containing solvents (e.g., acetone) could compete with the formation of the σ -hole interactions between molecules, slowing down crystallization. Solvents such as toluene could also influence the formation of crystals through the formation of π - π interactions. These thoughts, however, remain speculative though intriguing to pursue further.
- vii. While we do observe the polymorphs for 4, additional studies would help clarify lingering questions such as the abundance or if additional polymorphs may be present. Furthermore, the impact of solvents on the formation of the polymorphs would be useful to study. Screening of samples with powder X-ray diffraction would certainly help shed light on this matter.

ASSOCIATED CONTENT

Supporting Information

The Supporting Information is available free of charge at https://pubs.acs.org/doi/10.1021/acs.cgd.3c01485.

Background and rationalization of the project, additional commentary on specific interactions and brief summaries, liquid derivatives, crystalline voids, in silico studies, melting points and phase transitions, crystallographic tables and images, interactions and synthons, Crystal-Grower input files, DSC traces, NMR images, and computational output files (PDF)

AUTHOR INFORMATION

Corresponding Authors

Arsalan Mirjafari – Department of Chemistry, State University of New York at Oswego, Oswego, New York 13126, United

States; orcid.org/0000-0002-5502-0602; Email: Arsalan.Mirjafari@oswego.edu

Patrick C. Hillesheim — Department of Chemistry and Physics, Ave Maria University, Ave Maria, Florida 34142, United States; Occid.org/0000-0002-9567-4002; Email: Patrick.Hillesheim@avemaria.edu

Authors

Mairead Boucher – Department of Chemistry and Physics, Ave Maria University, Ave Maria, Florida 34142, United States

Sophia A. Bellia — Department of Chemistry and Physics, Ave Maria University, Ave Maria, Florida 34142, United States Alexis Howarth — Department of Chemistry and Physics, Ave Maria University, Ave Maria, Florida 34142, United States Anne Collart — Department of Chemistry and Physics, Ave

Maria University, Ave Maria, Florida 34142, United States;
o orcid.org/0000-0002-2964-880X

Muhammadiqboli Musozoda — Department of Chemistry, State University of New York at Oswego, Oswego, New York 13126, United States

Clinton Adu – Department of Chemistry, State University of New York at Oswego, Oswego, New York 13126, United States

Gary L. Guillet — Department of Chemistry, Furman University, Greenville, South Carolina 29613, United States Antonio Barbosa — Department of Chemistry and Physics, Ave Maria University, Ave Maria, Florida 34142, United States Pasquale F. Fulvio — School of Chemical and Biomolecular Engineering, Georgia Institute of Technology, Atlanta,

Georgia 30332, United States

Matthias Zeller — Department of Chemistry, Purdue
University, West Lafayette, Indiana 47907, United States;
orcid.org/0000-0002-3305-852X

Complete contact information is available at: https://pubs.acs.org/10.1021/acs.cgd.3c01485

Author Contributions

M.B., S.A.B., and A.H. contributed equally to this manuscript. All authors contributed to conceptualization, investigation, review, and editing. The project was designed by M.B., A.M., and P.C.H. Synthesis of the compounds was conducted by M.B., S.A.B., A.H., and A.C. NMR and DSC data were collected by M.M., C.A., and A.M. Crystallographic data were collected by P.C.H., G.L.G., and M.Z. Computational studies and crystallographic analysis were conducted by P.C.H. Viscosity and density modeling and discussion was done by P.F.F. P.C.H., A.M., and P.F.F. wrote the original draft of the manuscript. All authors have given approval to the final version of the manuscript prior to submission.

Funding

Acknowledgment is made to the donors of the American Chemical Society Petroleum Research Fund (66195-UNI10) for support of this research. Parts of this material are based upon work supported by the National Science Foundation through the Major Research Instrumentation Program under grant no. CHE 1530959 and 1919785.

Notes

The authors declare no competing financial interest.

ACKNOWLEDGMENTS

P.C.H. wishes to thank Florida Gulf Coast University for the use of their instrumentation. This work was supported by the Ave Maria University Department of Chemistry and Physics. A.M., M.M., and C.A. are grateful to the Richard S. Shineman Foundation and the Oswego College Foundation for their generous financial support.

REFERENCES

- (1) Beaujuge, P. M.; Fr, J. M. J. Molecular Design and Ordering Effects in π -Functional Materials for Transistor and Solar Cell Applications. *J. Am. Chem. Soc.* **2011**, *133*, 20009.
- (2) Desiraju, G. R. Crystal Engineering: A Holistic View. Angew. Chem., Int. Ed. 2007, 46 (44), 8342–8356.
- (3) Halcrow, M. A. Structure:Function Relationships in Molecular Spin-Crossover Complexes. *Chem. Soc. Rev.* **2011**, *40* (7), 4119.
- (4) Reichel, M.; Dosch, D.; Klapötke, T.; Karaghiosoff, K. Correlation between Structure and Energetic Properties of Three Nitroaromatic Compounds: Bis(2,4-Dinitrophenyl) Ether, Bis(2,4,6-Trinitrophenyl) Ether, and Bis(2,4,6-Trinitrophenyl) Thioether. J. Am. Chem. Soc. 2019, 141 (50), 19911–19916.
- (5) Dosch, D. E.; Reichel, M.; Born, M.; Klapötke, T. M.; Karaghiosoff, K. Investigation of Structure-Property Relationships of Three Nitroaromatic Compounds: 1-Fluoro-2,4,6-Trinitrobenzene, 2,4,6-Trinitrophenyl Methanesulfonate, and 2,4,6-Trinitrobenzaldehyde. *Cryst. Growth Des.* **2021**, *21* (1), 243–248.
- (6) Takise, R.; Muto, K.; Yamaguchi, J. Cross-Coupling of Aromatic Esters and Amides. *Chem. Soc. Rev.* **2017**, 46 (19), 5864–5888.
- (7) Sá, A. G. A.; de Meneses, A. C.; Araújo, P. H. H. d.; de Oliveira, D. A Review on Enzymatic Synthesis of Aromatic Esters Used as Flavor Ingredients for Food, Cosmetics and Pharmaceuticals Industries. *Trends Food Sci. Technol.* **2017**, *69*, 95–105.
- (8) Bocqué, M.; Voirin, C.; Lapinte, V.; Caillol, S.; Robin, J.-J. Petro-Based and Bio-Based Plasticizers: Chemical Structures to Plasticizing Properties. *J. Polym. Sci., Part A: Polym. Chem.* **2016**, *54* (1), 11–33.
- (9) Martin, A. D.; Britton, J.; Easun, T. L.; Blake, A. J.; Lewis, W.; Schröder, M. Hirshfeld Surface Investigation of Structure-Directing Interactions within Dipicolinic Acid Derivatives. *Cryst. Growth Des.* **2015**, *15* (4), 1697–1706.
- (10) Venkatesan, P.; Thamotharan, S.; Kumar, R. G.; Ilangovan, A. Invariant and Variable Intermolecular Interactions in Functionalized Malonic Acid Half-Esters: X-Ray, Hirshfeld Surface and PIXEL Energy Analyses. *CrystEngComm* **2015**, *17* (4), 904–915.
- (11) Shevchenko, A.; Serezhkin, V. Stereoatomic Model and Structure of Saturated Hydrocarbon Crystals. *Russ. J. Phys. Chem. A* **2004**, 78, 1598–1606.
- (12) Spackman, P. R.; Turner, M. J.; McKinnon, J. J.; Wolff, S. K.; Grimwood, D. J.; Jayatilaka, D.; Spackman, M. A. CrystalExplorer: A Program for Hirshfeld Surface Analysis, Visualization and Quantitative Analysis of Molecular Crystals. *J. Appl. Crystallogr.* **2021**, *54* (3), 1006–1011.
- (13) Blatov, V. A.; Shevchenko, A. P.; Proserpio, D. M. Applied Topological Analysis of Crystal Structures with the Program Package ToposPro. *Cryst. Growth Des.* **2014**, *14* (7), 3576–3586.
- (14) Lu, T.; Chen, F. Multiwfn: A Multifunctional Wavefunction Analyzer. J. Comput. Chem. 2012, 33 (5), 580–592.
- (15) Macrae, C. F.; Bruno, I. J.; Chisholm, J. A.; Edgington, P. R.; McCabe, P.; Pidcock, E.; Rodriguez-Monge, L.; Taylor, R.; van de Streek, J.; Wood, P. A. Mercury CSD 2.0 New Features for the Visualization and Investigation of Crystal Structures. *J. Appl. Crystallogr.* 2008, 41 (2), 466–470.
- (16) Yao, C.; Zhang, S.; Wang, L.; Tao, X. Recent Advances in Polymorph Discovery Methods of Organic Crystals. *Cryst. Growth Des.* **2023**, 23 (1), 637–654.
- (17) Gavezzotti, A. Chapter 2-The Intermolecular Chemical Bond: Physical Facts and Geometric Fiction. In *Theoretical and Computational Chemistry*; Gavezzotti, A., Ed.; Elsevier, 2021; Vol. 20, pp 25–52.

- (18) Apex3 V2019.1-0, SAINT V8.40A, 2019.
- (19) Krause, L.; Herbst-Irmer, R.; Sheldrick, G. M.; Stalke, D. Comparison of Silver and Molybdenum Microfocus X-Ray Sources for Single-Crystal Structure Determination. *J. Appl. Crystallogr.* **2015**, 48 (1), 3–10.
- (20) SHELXTL Suite of Programs, Version 6.14; Bruker Advanced X-Ray Solutions, 2000–2003.
- (21) Sheldrick, G. M. A Short History of SHELX. Acta Crystallogr., Sect. A: Found. Crystallogr. 2008, 64 (1), 112–122.
- (22) Sheldrick, G. M. Crystal Structure Refinement with SHELXL. Acta Crystallogr., Sect. C: Struct. Chem. 2015, 71 (1), 3-8.
- (23) Dolomanov, O. V.; Bourhis, L. J.; Gildea, R. J.; Howard, J. A. K.; Puschmann, H. OLEX2: A Complete Structure Solution, Refinement and Analysis Program. J. Appl. Crystallogr. 2009, 42 (2), 339–341.
- (24) Clydesdale, G.; Roberts, K. J.; Docherty, R. HABIT95 a Program for Predicting the Morphology of Molecular Crystals as a Function of the Growth Environment. *J. Cryst. Growth* **1996**, *166* (1–4), 78–83.
- (25) Macrae, C. F.; Sovago, I.; Cottrell, S. J.; Galek, P. T. A.; McCabe, P.; Pidcock, E.; Platings, M.; Shields, G. P.; Stevens, J. S.; Towler, M.; Wood, P. A. Mercury 4.0: From Visualization to Analysis, Design and Prediction. *J. Appl. Crystallogr.* **2020**, 53 (1), 226–235.
- (26) Bryant, M. J.; Rosbottom, I.; Bruno, I. J.; Docherty, R.; Edge, C. M.; Hammond, R. B.; Peeling, R.; Pickering, J.; Roberts, K. J.; Maloney, A. G. P. Particle Informatics": Advancing Our Understanding of Particle Properties through Digital Design. *Cryst. Growth Des.* 2019, 19 (9), 5258–5266.
- (27) Mayo, S. L.; Olafson, B. D.; Goddard, W. A. DREIDING: A Generic Force Field for Molecular Simulations. *J. Phys. Chem.* **1990**, 94 (26), 8897–8909.
- (28) Hill, A. R.; Cubillas, P.; Gebbie-Rayet, J. T.; Trueman, M.; de Bruyn, N.; Al Harthi, Z.; Pooley, R. J. S.; Attfield, M. P.; Blatov, V. A.; Proserpio, D. M.; Gale, J. D.; Akporiaye, D.; Arstad, B.; Anderson, M. W. CrystalGrower: A Generic Computer Program for Monte Carlo Modelling of Crystal Growth. *Chem. Sci.* **2021**, *12* (3), 1126–1146.
- (29) Anderson, M. W.; Gebbie-Rayet, J. T.; Hill, A. R.; Farida, N.; Attfield, M. P.; Cubillas, P.; Blatov, V. A.; Proserpio, D. M.; Akporiaye, D.; Arstad, B.; Gale, J. D. Predicting Crystal Growth via a Unified Kinetic Three-Dimensional Partition Model. *Nature* **2017**, 544 (7651), 456–459.
- (30) Stukowski, A. Visualization and Analysis of Atomistic Simulation Data with OVITO-the Open Visualization Tool. *Modell. Simul. Mater. Sci. Eng.* **2010**, *18* (1), 015012.
- (31) Zhao, Y.; Truhlar, D. G. The M06 Suite of Density Functionals for Main Group Thermochemistry, Thermochemical Kinetics, Noncovalent Interactions, Excited States, and Transition Elements: Two New Functionals and Systematic Testing of Four M06-Class Functionals and 12 Other Functionals. *Theor. Chem. Acc.* 2008, 120 (1–3), 215–241.
- (32) Chen, Z.; Rajamanickam, K. R.; Ding, M.; Kim, S. K.; Park, S.; Kim, E.; Lee, S.; Lee, T.-H. Discovery of PMSA Derivative 11 as a Novel Lead Compound for Therapeutic Treatment of Osteoporosis In Vitro and In Vivo. *J. Med. Chem.* **2023**, *66* (10), *6766*–*6781*.
- (33) Yu, Z.; Yao, H.; Xu, Q.; Liu, J.; Le, X.; Ren, M. Brønsted acid-catalyzed chlorination of aromatic carboxylic acids. *Phosphorus, Sulfur Silicon Relat. Elem.* **2021**, *196* (8), 685–689.
- (34) Howarth, A.; Barbosa, T. J.; Zeller, M.; Hillesheim, P. C. Pyridinium 3-Nitro-Benzoate 3-Nitro-Benzoic Acid (1/1). *IUCrData* **2021**, *6* (6), x210581.
- (35) Cruz-Cabeza, A. J.; Bernstein, J. Conformational Polymorphism. Chem. Rev. 2014, 114 (4), 2170-2191.
- (36) Spackman, M. A.; Jayatilaka, D. Hirshfeld Surface Analysis. CrystEngComm 2009, 11 (1), 19–32.
- (37) McKinnon, J. J.; Spackman, M. A.; Mitchell, A. S. Novel Tools for Visualizing and Exploring Intermolecular Interactions in Molecular Crystals. *Acta Crystallogr., Sect. B: Struct. Sci.* **2004**, *60* (6), 627–668.
- (38) Desiraju, G. R. Hydrogen Bridges in Crystal Engineering: Interactions without Borders. *Acc. Chem. Res.* **2002**, 35 (7), 565–573.

- (39) Price, S. S. L. Computed Crystal Energy Landscapes for Understanding and Predicting Organic Crystal Structures and Polymorphism. *Acc. Chem. Res.* **2009**, 42 (1), 117–126.
- (40) Sutradhar, D.; Chandra, A. K. Cl···Cl Halogen Bonding: Nature and Effect of Substituent at Electron Donor Cl atom. *ChemistrySelect* **2020**, *5* (2), 554–563.
- (41) Esrafili, M.; Solimannejad, M. A Theoretical Survey on Strength and Characteristics of F···F, Br···O and Br···Br Interactions in Solid Phase. *Phys. Chem. Res.* **2013**, *1* (2), 142–151.
- (42) Alkorta, I.; Elguero, J.; Frontera, A. Not Only Hydrogen Bonds: Other Noncovalent Interactions. *Crystals* **2020**, *10* (3), 180.
- (43) Vener, M. V.; Shishkina, A. V.; Rykounov, A. A.; Tsirelson, V. G. Cl···Cl Interactions in Molecular Crystals: Insights from the Theoretical Charge Density Analysis. *J. Phys. Chem. A* **2013**, *117* (35), 8459–8467.
- (44) Capdevila-Cortada, M.; Castelló, J.; Novoa, J. J. The nature of the C-Cl···Cl-C intermolecular interactions found in molecular crystals: a general theoretical-database study covering the 2.75–4.0 Å range. *CrystEngComm* **2014**, *16* (35), 8232–8242.
- (45) Capdevila-Cortada, M.; Novoa, J. J. The nature of the C−Br··· Br−C intermolecular interactions found in molecular crystals: a general theoretical-database study. *CrystEngComm* **2015**, *17* (17), 3354−3365.
- (46) Mazik, M.; Buthe, A. C.; Jones, P. G. C–H···Br, C–Br···Br, and C–Br··· π interactions in the crystal structures of mesitylene- and dimesitylmethane-derived compounds bearing bromomethyl units. *Tetrahedron* **2010**, *66* (1), 385–389.
- (47) Cavallo, G.; Metrangolo, P.; Milani, R.; Pilati, T.; Priimagi, A.; Resnati, G.; Terraneo, G. The Halogen Bond. *Chem. Rev.* **2016**, *116* (4), 2478–2601.
- (48) Dunitz, J. D. Organic Fluorine: Odd Man Out. ChemBioChem **2004**, 5 (5), 614–621.
- (49) Siram, R. B. K.; Karothu, D. P.; Guru Row, T. N.; Patil, S. Unique Type II Halogen...Halogen Interactions in Pentafluorophen-yl-Appended 2,2′-Bithiazoles. *Cryst. Growth Des.* **2013**, *13* (3), 1045–1049.
- (50) Lo, R.; Ballabh, A.; Singh, A.; Dastidar, P.; Ganguly, B. Probing the O···Br—Br halogen bonding in X-ray crystal structures with ab initio calculations. *CrystEngComm* **2012**, *14* (5), 1833—1841.
- (51) Nayak, S. K.; Terraneo, G.; Forni, A.; Metrangolo, P.; Resnati, G. C–Br···O supramolecular synthon: in situ cryocrystallography of low melting halogen-bonded complexes. *CrystEngComm* **2012**, *14* (13), 4259–4261.
- (52) Batsanov, S. S. Van Der Waals Radii of Elements. *Inorg. Mater.* **2001**, *37* (9), 871–885.
- (53) Murray, J. S.; Lane, P.; Politzer, P. Expansion of the σ -Hole Concept. *J. Mol. Model.* **2009**, *15* (6), 723–729.
- (54) Bissantz, C.; Kuhn, B.; Stahl, M. A Medicinal Chemist's Guide to Molecular Interactions. J. Med. Chem. 2010, 53 (14), 5061–5084.
- (55) Desiraju, G. R.; Vittal, J. J.; Ramanan, A. *Crystal Engineering*; Co-Published with Indian Institute of Science (IISc): Bangalore, India, 2011.
- (56) Jha, K. K.; Yadav, Y.; Srivastava, S. B.; Chakraborty, D.; Johari, P.; Singh, S. P.; Munshi, P. Structure-Property Relationship in an Organic Semiconductor: Insights from Energy Frameworks, Charge Density Analysis, and Diode Devices. *Cryst. Growth Des.* **2019**, *19* (5), 3019–3029.
- (57) Mackenzie, C. F.; Spackman, P. R.; Jayatilaka, D.; Spackman, M. A. CrystalExplorer Model Energies and Energy Frameworks: Extension to Metal Coordination Compounds, Organic Salts, Solvates and Open-Shell Systems. *IUCrJ* 2017, 4 (5), 575–587.
- (58) Price, S. L. Predicting Crystal Structures of Organic Compounds. *Chem. Soc. Rev.* **2014**, 43 (7), 2098–2111.
- (59) Hartman, P.; Bennema, P. The Attachment Energy as a Habit Controlling Factor: I. Theoretical Considerations. *J. Cryst. Growth* **1980**, 49 (1), 145–156.
- (60) Docherty, R.; Clydesdale, G.; Roberts, K. J.; Bennema, P. Application of Bravais-Friedel-Donnay-Harker, Attachment Energy

and Ising Models to Predicting and Understanding the Morphology of Molecular Crystals. *J. Phys. Appl. Phys.* **1991**, 24 (2), 89–99.

- (61) Jin, L.-F.; Xiao, F.-P. Methyl 3-Nitrobenzoate. Acta Crystallogr., Sect. E: Struct. Rep. Online 2005, 61 (5), o1237-o1238.
- (62) Matheson, A. J. The Influence of Molecular Rotation on Transport Processes in Liquids. *Adv. Mol. Relax. Process.* **1972**, 3 (1–4), 153–158.
- (63) Casalini, R.; Bair, S. The Inflection Point in the Pressure Dependence of Viscosity under High Pressure: A Comprehensive Study of the Temperature and Pressure Dependence of the Viscosity of Propylene Carbonate. *J. Chem. Phys.* **2008**, *128* (8), 084511.
- (64) Jankowiak, A.; Januszko, A.; Ringstrand, B.; Kaszynski, P. A New Series of Nematic and Smectic Liquid Crystals with Negative Dielectric Anisotropy: The Effect of Terminal Chain Substitution on Thermal and Electro-optical Properties. *Liq. Cryst.* **2008**, *35* (1), 65–77.